Dyes and Pigments 94 (2012) 247–257

Contents lists available at SciVerse ScienceDirect

Dyes and Pigments

journal homepage: www.elsevier.com/locate/dyepig

Simple strategies towards bright polymer particles via one-step staining procedures

Thomas Behnke, Christian Würth, Eva-Maria Laux, Katrin Hoffmann, Ute Resch-Genger*

BAM Federal Institute for Materials Research and Testing, Richard-Willstaetter-Str. 11, 12489 Berlin, Germany

ARTICLE INFO

Article history:
Received 14 September 2011
Received in revised form
19 January 2012
Accepted 21 January 2012
Available online 28 January 2012

Keywords:
Fluorescence
Polystyrene
Particles
Encapsulation
Quantum yield
Zeta potential

ABSTRACT

In order to develop simple and versatile procedures for the preparation of red emissive particles, various one-step swelling procedures for the loading of fluorophores into nanometer- and micrometer-sized polystyrene particles were systematically assessed. Parameters studied for model dyes from common dye classes include the composition of the swelling medium, dye charge and polarity, dye concentration, and particle surface chemistry. The dye loading procedures were compared based upon the efficiency of dye incorporation, fluorescence intensity, and colloidal stability of the resulting particles as well as the absence of dye leaking as determined by absorption and fluorescence spectroscopy, flow cytometry, and measurements of zeta potentials. In addition, for the first time, the influence of the amount of incorporated dye on the absolute fluorescence quantum yield and brightness of the fluorescent particles was investigated for selected chromophores in differently sized particles using a custom-made calibrated integrating sphere setup. Our results demonstrate the general suitability of these one-step loading procedures for efficient particle staining with neutral, zwitterionic, and charged fluorophores like oxazines, coumarines, squaraines, xanthenes, and cyanines emitting in the visible and near infrared. Dye polarity was identified as a suitable tool to estimate the loading efficiency of fluorophores into these polymer particles.

1. Introduction

The design and characterization of fluorescent nano- and micrometer-sized particles for biological, diagnostic, and photonic applications present a very active research area [1–9]. This includes versatile platforms for fluorescence assays, nanosensors and contrast agents for bioimaging, optical barcoding, and optically active materials [10–15]. In the last years, there evolved an increasing interest in bright fluorophores with emission in the near infrared region (NIR) that often requires dye encapsulation to enhance the generally lower fluorescence quantum yields and chemical stabilities of NIR dyes and to overcome their often reduced water solubility [16–24].

Accordingly, there is a considerable need for simple, flexible, and reproducible procedures for the preparation of differently sized fluorescent particles from organic or inorganic fluorophores that can be used for a broad variety of fluorophores from different dye classes with emission in the visible and NIR region. Moreover, these synthetic strategies should enable the incorporation of dye combinations for multiplexied detection schemes and barcoding schemes and the combination of fluorophores with magnetic or radioactive compounds for applications in bead-based sedimentations assays, as magneto-optical sensors or as multimodal contrast agents for combined functional and anatomically imaging of pathological changes [25,26]. For the eventually desired prediction of appropriate procedures for the straightforward incorporation of new fluorophores and, even more challenging, the spectroscopic properties of the resulting particles, systematic studies are required to derive suitable tools and to identify structure–property relationships. Of special importance is here the estimation of the particle brightness that determines the signal size from the chromophore site [27].

Principally, fluorescent particles can be prepared by labeling of surface-functionalized particles with fluorophores [28], staining of polymer particles with non-reactive dyes [29–32], steric inclusion during particle formation, and, synthetically more challenging, synthesis from dye-labeled monomers or precursors [33,34]. The first approach yields freely accessible fluorophores not protected by a matrix from undesired interactions with abundant plasma proteins in the case of in vitro and in vivo applications and can favor

* Corresponding author. Tel.: +49 3081041134; fax: +49 3081041157.
E-mail address: ute.resch@bam.de (U. Resch-Genger).

0143-7208/$ – see front matter © 2012 Elsevier Ltd. All rights reserved.
doi:10.1016/j.dyepig.2012.01.021

fluorescence quenching dye–dye interactions, especially at high labeling densities [35,36]. Except for particle staining, these synthetic strategies require either expensive reactive dyes or higher temperatures or the presence of radicals during, e.g., the polymerization. Such stringent reaction conditions can hamper the encapsulation of fluorophores of limited chemical stability as found for many red emissive dyes.

A facile route to micro- and nanoparticles with emission in the visible (vis) and near-infrared (NIR) presents the staining of commercial polymer particles like poly(methyl methacrylate) (PMMA) [29] or polystyrene [30–32,37] particles via swelling procedures [38–42]. Especially attractive are polystyrene particles (PSP) because they are commercially available in different sizes ranging from 15 nm up to several micrometers with a narrow size distribution and various surface chemistries. Moreover, polystyrene is generally considered as inert and non-toxic [43–49]. Although staining of PSP has been frequently reported [50–54], typical dye loading protocols require several preparation steps and different solvents, rendering them unnecessarily tedious. To render staining procedure more efficient, single step procedures are mandatory. Moreover, for the straightforward staining of PSP with dyes from different dye classes and thus, e.g., varying rigidity, chromophore charge, and hydrophilicity, tools are mandatory that enable the prediction of suitable procedures preferably from some simply accessible dye-inherent physico-chemical property.

In order to develop versatile and efficient one-step protocols for the encapsulation of vis and NIR fluorophores, we systematically investigated swelling procedures for nano- and micrometer-sized PSP of various surface chemistry and fluorophores varying in chromophore charge, size, polarity, and hydrophilicity. Dyes studied range from water-soluble anionic cyanines like DY-676 and DY-751 over squaraines, xanthenes, and oxazines like the neutral polarity probe Nile Red to hydrophobic heptamethines with a positively charged chromophore. In a first step, different loading strategies were compared with respect to dye incorporation efficiency, thereby aiming to identify tools for the prediction and tuning of the fluorophore loading behavior. In a second step, the physico-chemical properties of the resulting dye-loaded particles were assessed. Here, special emphasis was dedicated to the influence of dye type, charge, and concentration on the application-relevant optical features of these particles including the absolute fluorescence quantum yield and the zeta potential as a measure for colloidal stability. The ultimate goals were here to identify physico-chemical quantities of dyes that enable the predicition of suitable loading procedures and to derive the influence of fluorophore charge and content, particle size, and particle surface chemistry on the application-relevant spectroscopic properties of stained PSP and their stability as a prerequisite for bright particles.

2. Material and methods

2.1. Materials

Carboxyl-functionalized and non-functionalized plain polystyrene particles with sizes of 25 nm, 50 nm, 100 nm, 1 μm, and 8 μm were purchased from Kisker Biotech GmbH and 100 nm sized amino-functionalized latex particles from Micromod GmbH. According to the particle manufacturers, the amount of surface groups was about 140 nmol/mg for aminated PSP, and 180 nmol/mg for carboxylated PSP. All particles were ultrasonically treated prior to use. Nile Red, Coumarin 153, and Rhodamine 101 were obtained from Fluka GmbH, the DY-dyes from Dyomics GmbH, Itrybe from Otava Ltd, and Square-730 (Sq-730) from Seta BioMedicals. All dyes were employed without further purification. All solvents (tetrahydrofuran (THF), dimethylformamide (DMF), chloroform, 2-propanol, dibutylether (BOB) and ethanol) that were of spectroscopic grade, were purchased from Sigma–Aldrich Co. 4-(2-hydroxyethyl)-1-piperazineethanesulfonic acid (HEPES), Hanks' Balanced Salt Solution (HBSS) and bovine serum albumin (BSA) were obtained from Sigma–Aldrich Inc. Sheath fluid® used for the preparation of the PSP suspensions for the flow cytometric studies was purchased from Partec GmbH. All solvents were used as received.

2.2. Methods

2.2.1. Swelling procedures

The dyes were dissolved in THF or DMF in different concentrations ranging from 5×10^{-3} mol/L to 5×10^{-5} mol/L. Dye loading of the PSP was performed by addition of 100 μL of a dye-containing solution to 600 μL of an aqueous suspension of the PSP (0.5 weight percent (w%)). Particles <100 nm were incubated for 30 min, larger particles for 1 h, before another 800 μL water were added and the occasionally shaken suspension was centrifuged (Eppendorf centrifuge 5415D: 100 nm PSP at 15,000 *g* for 40 min, 1 μm PSP at 5000 *g* for 10 min, and 8 μm PSP at 4000 *g* for 10 min; Beckman Coulter centrifuge Avanti J-20 XP: 50 nm PSP at 45,000 *g* for 45 min and 25 nm PSP at 75,000 *g* for 45 min). The separated PSP were washed twice with bidistilled water followed by resuspension in bidistilled water in an ultrasonic bath.

For selected fluorophores, dye loading was also carried out in chloroform, substituting THF or DMF. In this case, prior to the addition of the dye-containing solution, the commercial aqueous suspensions of PSP were centrifuged and washed twice with 2-propanol to remove water.

For the investigation and optimization of the swelling conditions with respect to the amount of incorporated dye, different stock solutions of the fluorophores were prepared to assure an amount of dye of 1×10^{-7} mol per sample, regardless of the volume fraction of the solvent employed. In the case of Sq-730 and the DY-dyes, an amount of dye equaling 1×10^{-8} mol per sample was used, due to their reduced solubility and increased aggregation tendency. The dye solutions were added to the particle suspensions, each containing 3 mg of 1 μm PSP.

For studies focusing on the influence of the pH during the staining procedure, the pH value of the staining solution was adjusted with 1 mol/L HCl or NaOH. In the case of time-dependent swelling studies, 1 μm PSP were used. Here, the end of the centrifugation process was assumed to be the end of the dye incorporation process, since at this point, the contact between the PSP and the dye-containing supernatant is limited.

2.2.2. Determination of the amount of incorporated dye

For the determination of the amount of PSP-incorporated dye, the PSP suspensions were centrifuged as previously described and the supernatant was removed. The PSP were dissolved in THF, followed by subsequent measurements of the absorption spectra of the THF solutions. The average amount of dye, incorporated into 3 mg PSP employed for the dye loading studies, was calculated from the absorbance measured at the dye's longest wavelength absorption maximum, using the Beer–Lambert law and the molar absorption coefficient of the dye, previously determined in THF in the presence of 0.1 w% dissolved polystyrene. The relative amount of encapsulated dye (degree of dye loading) equals the quotient of the applied and the actually incorporated amount of fluorophore molecules. The reproducibility of this method was determined by dissolving aliquots of identical size, i.e., volume and particle concentration, from seven different batches of stained particles, yielding a relative standard deviation of 8% for the resulting dye concentrations.

2.2.3. Leaking studies

A total of 1 μm-sized carboxylated PSP, stained with either Nile Red or Itrybe (1×10^{-7} mol), were suspended in bidistilled water resulting in 0.1 w% aqueous particle suspensions. One fraction of the suspension was used to determine the amount of incorporated dye. The other fraction was kept in the dark at room temperature (298 ± 1 K) for one year simulating typical storage conditions. Leaking studies were also performed in HBSS containing 5 w% bovine serum albumin (BSA; HBSS/BSA) modelling a biologically relevant environment. For this purpose, 0.1 w% suspensions of 100-nm sized PSP stained with Itrybe and Nile Red, respectively, were kept for four weeks in HBSS/BSA at room temperature in the dark. Subsequently, all samples were centrifuged and the supernatant was separated and evaporated. The residues were dissolved in 1.5 mL ethanol and the absorption spectra of these solutions were measured in semi-micro cuvettes.

2.2.4. Absorption and fluorescence spectroscopy

Prior to each spectroscopic measurement, the washed PSP were suspended in bidistilled water, yielding a polystyrene concentration of 0.1 w%. These suspensions were transferred to 4 mm semi-micro PMMA cuvettes (Brand).

Absorption measurements. Absorption measurements were carried out with a Cary 5000 UV–Vis–NIR spectrophotometer from Varian Inc. at room temperature. For the determination of the molar absorption coefficients of the fluorophores in THF in the presence of 0.1 w% polystyrene, the absorption spectra of different dye concentrations, originating from at least two stock solutions, were measured. The dye concentration was varied from 5×10^{-6} mol/L to 1×10^{-5} mol/L. In all cases, 1-cm quartz cuvettes (Hellma) were used.

Fluorescence measurements. Fluorescence measurements were performed with a calibrated Spectronics Instruments 8100 spectrofluorometer equipped with Glan Thompson polarizers in the excitation and emission channel in a 0°/90° standard measurement geometry. The excitation polarizer was set to 0° and the emission polarizer to 54.7°. The resulting emission spectra were corrected for the spectral responsivity of the fluorometer's emission channel as previously described [55]. For all spectroscopic measurements, the temperature was kept constant at (298 ± 1) K.

Reabsorption effects that depend on the dye- and matrix-specific Stokes shift and on dye concentration, see Supporting Information (SI), Figure 1S, were minimized by using dilute suspensions and short optical pathlengths.

2.2.5. Absolute fluorescence quantum yields

The absolute fluorescence quantum yields (Φ_f) of selected dyes and dye-stained PSP that equal the number of emitted photons (N_{em}) per absorbed photons (N_{abs}), were determined with a custom-designed calibrated integrating sphere setup. This setup consists of a xenon lamp coupled to a single monochromator and a six inch Spectraflect-coated integrating sphere (Labsphere GmbH) coupled with a quartz fiber to an imaging spectrograph (Shamrock 303i, Andor Inc.) equipped with a Peltier-cooled thinned back side-illuminated deep depletion charge coupled device. A reference detector was implemented into the setup to account for fluctuations of the radiant power reaching the sample. The sample or blank (i.e., the pure solvent) in a conventional 1-cm quartz cell was mounted into the center of the integrating sphere. The excitation light was focused into the middle of the sample. The absolute fluorescence quantum yield was calculated from the measured spectrally corrected signals of the blank (I_{CB}) and the sample (I_{CS}) according to Eq. (1) [56].

$$\Phi_f = \frac{\int_{\lambda_{em_1}}^{\lambda_{em_2}} \frac{\lambda_{em}}{hc}(I_{CS}(\lambda_{em}) - I_{CB}(\lambda_{em}))d\lambda_{em}}{\int_{\lambda_{ex_1}}^{\lambda_{ex_2}} \frac{\lambda_{ex}}{hc}(I_{CB}(\lambda_{ex}) - I_{CS}(\lambda_{ex}))d\lambda_{ex}} = \frac{N_{em}}{N_{abs}} \quad (1)$$

For dyes displaying a considerable spectral overlap between absorption and emission, the measured fluorescence quantum yields were corrected for reabsorption effects [57].

2.2.6. Zeta potential

All measurements were carried out at (298 ± 1) K with a Malvern Zeta Nanosizer. This instrument uses a 4 mW He–Ne laser (633 nm) and a scattering angle of 173°. The zeta potentials of the suspensions containing 0.1 w% PSP, were calculated from the measured electrophoretic mobilities using the Smoluchowski relation, which is valid for aqueous solutions containing low electrolyte concentrations [58]. To ensure a constant pH and electrolyte concentrations, all suspensions used contained 0.1 mM HEPES at pH 7 if not otherwise stated.

2.2.7. Flow cytometry

Flow cytometry measurements were carried out at (298 ± 1) K with a Partec CyFlow instrument equipped with a 20 mW, 488 nm solid state laser. This laser was used for the measurement of both particle fluorescence and frontside scattering (FSC), which is related to particle size. The fluorescence was detected in a spectral window of 565–615 nm (bandpass filter). All particle suspensions were diluted in Sheath fluid® yielding PSP concentrations of 0.001 w%.

2.2.8. Fluorescence microscopy

Confocal laser scanning microscopy (CLSM) using an Olympus FV1000 was employed to judge the homogeneity of PSP staining, see SI.

2.2.9. Calculation of log D values

The log *D* values used as a measure for dye polarity were calculated with the calculator plugin for structure property prediction and calculation, Marvin 5.4.0.1, 2010, ChemAxon (http://www.chemaxon.com). For compounds with (de)protonable groups, log *D* values are pH-dependent, representing the distribution of the dye and its (de)protonated species in an 1-octanol/water mixture at a certain pH, see also Eq. (2). Here, c_{Oct} and c_{Water} equal the sum of the concentrations of all existing species. For the log *D* calculations, we used a pH of 5.5 if not otherwise stated.

$$\log D = \frac{\sum_1^n c_{Oct}^n}{\sum_1^n c_{Water}^n} \quad (2)$$

3. Results and discussion

Facile one-step swelling procedures provide the most direct access to micro- and nanometer-sized particles with customized emission characteristics and surface functionalities. Desired features, that are studied in this work, are an efficient sterical incorporation, preservation of the surface functionalities and the size and size distribution of the particles, a high fluorescence quantum yield of the encapsulated fluorophores, and a good colloidal stability of the resulting particles.

3.1. Optimization of staining conditions

In order to optimize and generalize the conditions of our swelling procedures, several parameters affecting dye encapsulation were studied including the polarity and composition of the solvent system or swelling medium and the swelling time. Suitable staining media should lead to swelling of the polymer matrix without dissolving it in a short period of time and enable the preparation of highly concentrated dye solutions for efficient dye loading. Solvent systems assessed here based on incorporation studies with 1-μm sized carboxy-functionalized PSP and different model dyes were THF/water, DMF/water, and chloroform/2-propanol. THF, DMF, and chloroform were chosen as they present common solvents for many different fluorophores. As model dyes, we used the neutral oxazine Nile Red, a well studied polarity probe, displaying environment-sensitive absorption and emission spectra [59–62], the cationic heptamethine Itrybe, with spectral properties barely affected by dye environment, the zwitterionic NIR-emissive squaraine dye Sq-730, and the negatively charged pentamethine DY-750, an NIR dye equipped with a carboxylic and a sulfonic acid group. Particle loading was evaluated based upon the measured degree of dye loading (see Section 2.2.2), flow cytometry, and confocal laser scanning microscopy (see SI). Flow cytometry enables the characterization of the stained particles on a single particle level with respect to changes in particle size or size distribution, exploiting the intensity of the FCS signal, and a comparison of their relative fluorescence intensity. Fluorescence microscopy was employed to judge the homogeneity of PSP staining.

The influence of the swelling time and solvent composition on the relative fraction of incorporated fluorophores is shown in Fig. 1 for mixtures of THF and water and the dyes Nile Red (left) and Itrybe (right). In the case of Nile Red, dye encapsulation was basically completed within 15 min, and for Itrybe, after 30 min. This suggests a slower diffusion rate of the larger cationic chromophore Itrybe into the polymer matrix. For both dyes, optimum loading results are obtained with a volume fraction of 14% THF. PSP staining does not affect the size and size distribution of the initial PSP as revealed by flow cytometry comparing the FSC signal for blank and 5×10^{-8} mol Nile Red-stained PSP shown in Fig. 2 and DLS data (not shown). All PSP are homogeneously stained according to confocal laser scanning microscopy (see SI, Figure 2S).

Volume fractions of THF below 14% barely affect the relative amount of incorporated Nile Red. In contrast, for the larger cationic dye Itrybe, the degrees of dye loading are reduced (Fig. 1). This is attributed to precipitation of the water-insoluble fluorophore in the polar solvent system. It cannot be excluded that in the case of Nile Red, low THF concentrations may also favor dye precipitation and adsorption onto PSP that could not be distinguished from incorporated dye molecules with our method of analysis. Volume fractions of THF exceeding 14% lead to a decrease in the amount of incorporated dyes (Fig. 1). This is ascribed to the good solubility of both fluorophores in THF, reducing the driving force for dye diffusion into PSP. For THF fractions exceeding 30%, the PSP start to dissolve as indicated by the shift of the intensity of the FSC signals to lower intensities (Fig. 2).

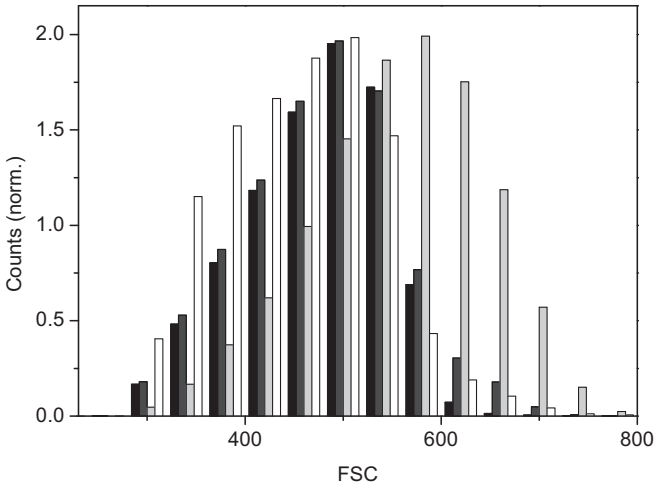

Fig. 2. Flow cytometry data comparing the intensity of the FSC signal from 1 μm-sized carboxylated blank PSP (black bars) and the corresponding PSP stained with 5×10^{-8} mol of Nile Red (dark grey bars). Use of a THF fraction of 30% (white bars) results in partially dissolved PSP. Addition of 0.1 mol/L phosphate buffer (light grey bars) leads to agglomeration (see also Section 3.6 and Table 2) as indicated by the increasing FSC signal intensity.

For the encapsulation of certain squaraines and cyanine dyes with limited solubility in THF, also other swelling solvent mixtures were tested, like chloroform/2-propanol and DMF/water. As shown in Fig. 3, we could accomplish relatively high degrees of dye loading in the case of DY-750 and moderate ones for Sq-730, using only small fractions of the dye-containing organic solvents DMF and chloroform. This is ascribed to the decreased solubility of these dyes in the respective swelling mixture, increasing the driving force for dye diffusion into the polystyrene matrix. For staining media containing more than 95% water or 2-propanol, no dye incorporation was observed, either due to a lack of swelling of the matrix or

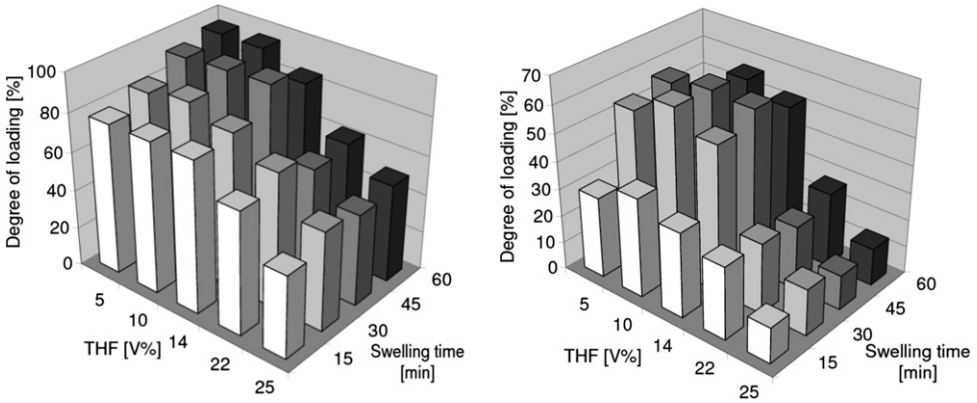

Fig. 1. Degree of dye loadings (left panel: Nile Red; right panel: Itrybe) of 1-μm sized carboxylated PSP as a function of the volume fraction of THF in the swelling solution and the swelling time. The amount of dye in the swelling solution was kept constant at 1×10^{-7} mol.

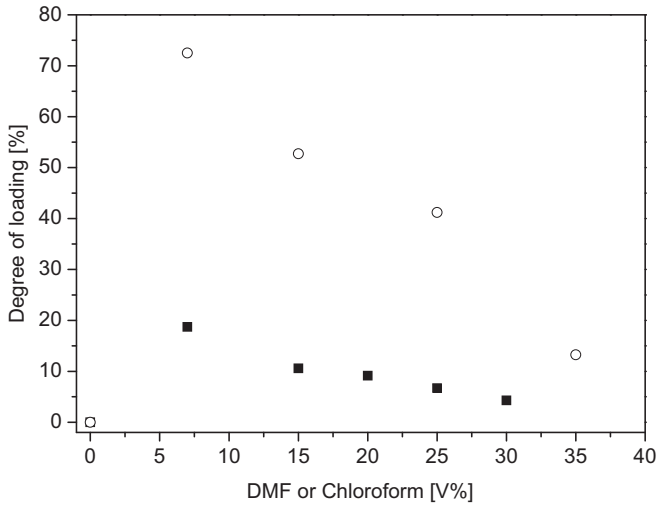

Fig. 3. Degree of loadings of Sq-730 (full squares) and DY-750 (open circles) in carboxylated PSP (1 μm) as a function of the volume fraction of chloroform in 2-propanol (Sq-730) or the volume fraction of DMF in water (DY-750) in the swelling solution.

less likely, to instant precipitation of the dye, following the addition to the aqueous or isopropanolic PSP suspension.

The results obtained with the different swelling media using a constant volume fraction of the dye-containing solvent, i.e., THF, DMF or chloroform, are summarized for our model dyes Nile Red (neutral oxazine), Itrybe (cationic cyanine), Sq-730 (zwitterionic squaraine at the chosen pH), and DY-750 (anionic cyanine) in Fig. 4. Obviously, with these swelling mixtures, we could identify procedures applicable for the encapsulation of the most important classes of NIR fluorophores into PSP without altering the initial particle size. THF/water seems to be best suited for Nile Red and Itrybe yielding degrees of loading of at least 50%. DMF/water is a good choice for the cyanines Itrybe and DY-750 and only in the case of Sq-730, optimum results were obtained with chloroform/2-propanol. Apparently, the balance between fluorophore solubility in the staining medium used for PSP swelling as compared to its solubility in the polystyrene matrix, i.e., the dye partition coefficient, is the most important parameter, controlling the efficiency of dye incorporation, leaving the swelling of the polystyrene matrix only subordinate and hampering staining for very low fractions of swelling solvent.

3.2. Concentration-control of dye loading

In order to optimize dye loading and to identify a tool for the control and prediction of its efficiency, we investigated the correlation between the amount of applied dye in the different swelling media and the amount of incorporated dye for Nile Red, Itrybe, Sq-730, and DY-750. The fraction of encapsulated dye was determined by dissolution of the stained particles (see Section 2.2.2). Fig. 5 summarizes the results obtained for the THF/water swelling medium and a concentration range of 1×10^{-6} mol/L up to 1×10^{-3} mol/L of applied dye. In most cases, we found a linear concentration dependence that enables straightforward control of the amount of encapsulated fluorophores. A similar behavior was observed for the other swelling systems. Such a linear correlation is a prerequisite for the simple optimization of particle fluorescence and brightness as detailed in a following section. For Nile Red and Itrybe showing a good solubility in the dye-containing solvent, we further increased the dye concentration up to 5×10^{-7} mol/L. This seems to lead to a saturation of the PS matrix, as suggested by the reduced degree of loading (Fig. 5).

3.3. Incorporation efficiency and hydrophilicity

Searching for parameters to predict the dye loading efficiency into PSP, we investigated the suitability of the log D value (see Section 2.2.9). For staining with fluorophores from different dye classes varying in charge and size, a 14% DMF/water mixture was employed, since DMF presents an excellent solvent for many chemically different chromophores. For the log D calculations, we used a pH of 5.5 present in the staining solutions containing 0.1 w% 1-μm sized carboxylated PSP.

As follows from Fig. 6, revealing a linear correlation between the degree of dye loading and the log D value for the dye-solvent system studied, the log D value presents an excellent tool for the prediction of the incorporation efficiency of fluorophores ranging from water-soluble anionic dyes with three acid groups (DY-676 and DY-751) up to hydrophobic heptamethine Itrybe. For

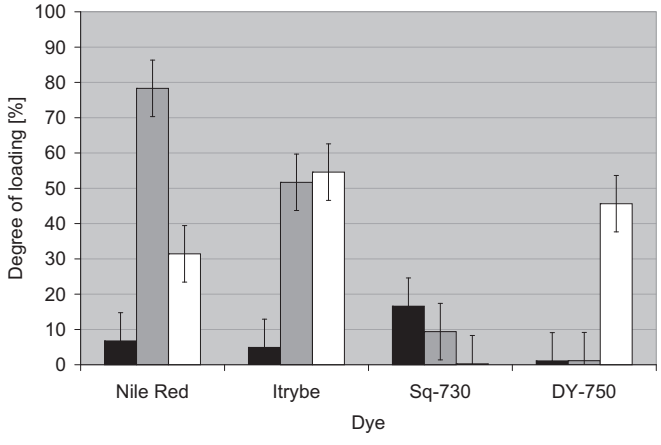

Fig. 4. Degree of dye loadings of carboxylated PSP (1 μm) with four model dyes from different dye classes determined for the staining systems chloroform/2-propanol (black bars), THF/water (grey bars), and DMF/water (white bars); the volume fraction of the dye-containing solvent, chloroform, THF or DMF, respectively, was kept constant at 14%.

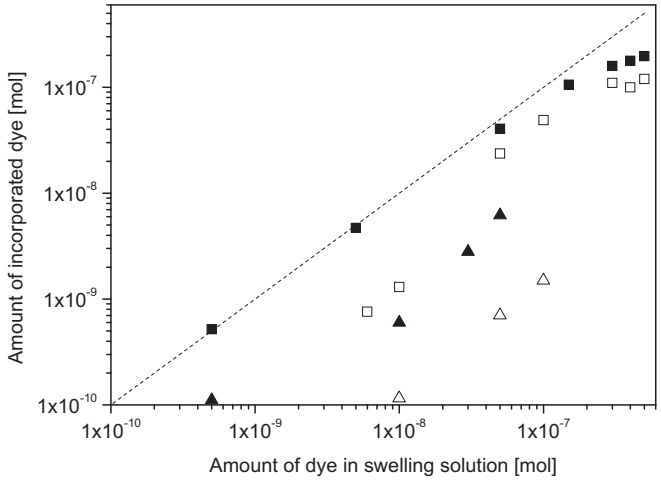

Fig. 5. Amount of incorporated dye in 1-μm sized carboxylated PSP as a function of the amount of fluorophore in the swelling solution (14% THF/water) for Nile Red (full squares), Sq-730 (full triangles), Itrybe (open squares), and DY-750 (open triangles). The dashed line represents the theoretical incorporation of 100% dye.

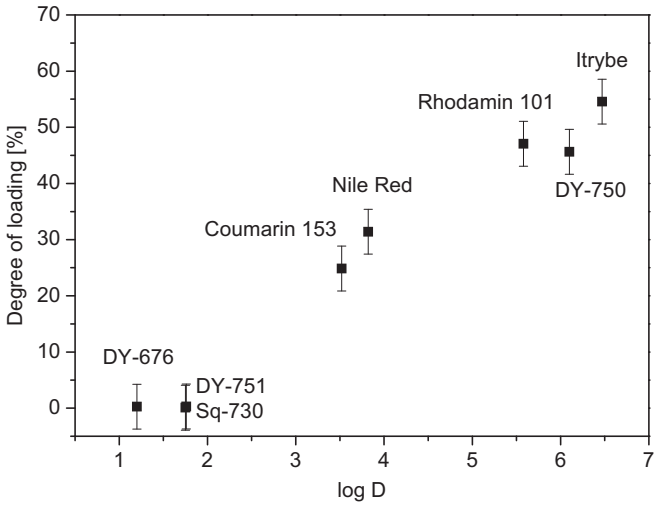

Fig. 6. Degree of dye loadings of common vis and NIR fluorophores in PSP as a function of $\log D$ (pH 5.5) for 1-μm sized carboxylated PSP. The amount of dye applied was 5×10^{-8} mol in a 14% DMF/water staining solution.

hydrophilic dyes with $\log D < 2$, only very small degrees of dye loading <5% can be achieved with. For these fluorophores, the staining efficiency can be improved using a less polar staining medium like THF/water that enhances the diffusion of the dye molecules from the solvent mixture into PS (see Figures 3 and 4). Dyes with $\log D < 1$ are usually not incorporated into PSP, regardless of the solvent system used.

3.4. Influence of particle size

In order to derive a possible influence of particle size and thus surface-to-volume ratio on the amount of incorporated dye for our swelling procedures, we performed loading studies with PSP of sizes ranging from 25 nm to 8 μm and the representative hydrophilic and hydrophobic dyes Sq-730 ($\log D = 1.8$) and Itrybe ($\log D = 5.6$) using our previously optimized swelling protocols (Fig. 1; THF content of 14%, 5×10^{-4} mol/L of Itrybe and 1×10^{-4} mol/L of Sq-730 used for 3 mg PSP). In the case of Itrybe, we observed an excellent correlation between the amount of fluorophore in the swelling solution and in the PSP, independent of particle size (see SI, Figure 3S). For Sq-730, however, the degree of dye loading depends on particle size. Apparently, for a constant mass of 3 mg PSP, the amount of incorporated dye increases with increasing surface-to-volume ratio (for the given timeframe). This is ascribed to the lower diffusion rate of this polar dye into the PS matrix. Accordingly, a larger surface enhances the incorporation process. In the case of a more hydrophobic dye like Itrybe revealing a higher diffusion rate, the influence of the surface area does not seem to be crucial.

3.5. pH-Tuning of the degree of dye loading

Hydrophilic dyes carrying more than a single carboxylic or sulfonic acid usually show low incorporation efficiencies at pH of >5 present in the PSP suspension where both types of acid groups are deprotonated. The fluorophore's hydrophobic character, however, can be tuned by altering the pH of the staining suspension, thereby inducing protonation of all or at least some of these groups, depending on the corresponding pK_a values. Fig. 7 summarizes the influence of pH on the $\log D$ value and the amount of incorporated dye for two cyanines differing only in the number of the sulfonic acid groups attached to the chromophore (DY-750: one COOH group, one SO_3H group; DY-751: one COOH group, two SO_3H groups) and the cyanine Itrybe containing no protonable substituents. Interestingly, DY-750 reveals a degree of dye loading of 26% even at pH values where all acid functions are expected to be deprotonated. With decreasing pH, the carboxylate groups of DY-750 and DY-751 become protonated as reflected by an increasing $\log D$ that is accompanied by an increase of the amount of incorporated dye at pH 7 compared to pH 4. Further enhancement of the incorporation of DY-751 observed at pH 2 ($\log D > 6$) can suggest partial protonation of the dye's sulfonate groups although in the case of DY-750, the degree of dye loading is not altered. In contrast, incorporation of our control Itrybe, studied at pH 4, 7.5 and 10.5, is independent of pH (Fig. 7, right panel). The strong increase in the amount of PSP-incorporated fluorophores observed for DY-751 and the considerable differences between DY-750 and DY-751 despite their similar chromophore systems emphasize the considerable potential of pH-controlled staining. Similarly, this underlines the need for a proper choice of the pH of the staining medium for fluorophores containing acid or amino functionalities.

In a second step, we investigated the influence of common surface functionalities of PSP, i.e., plain, carboxylated, and aminated, on dye loading of 100-nm sized PSP at three pH values for differently charged dyes with pH-insensitive and pH-dependent $\log D$ values. This included neutral Nile Red and cationic Itrybe

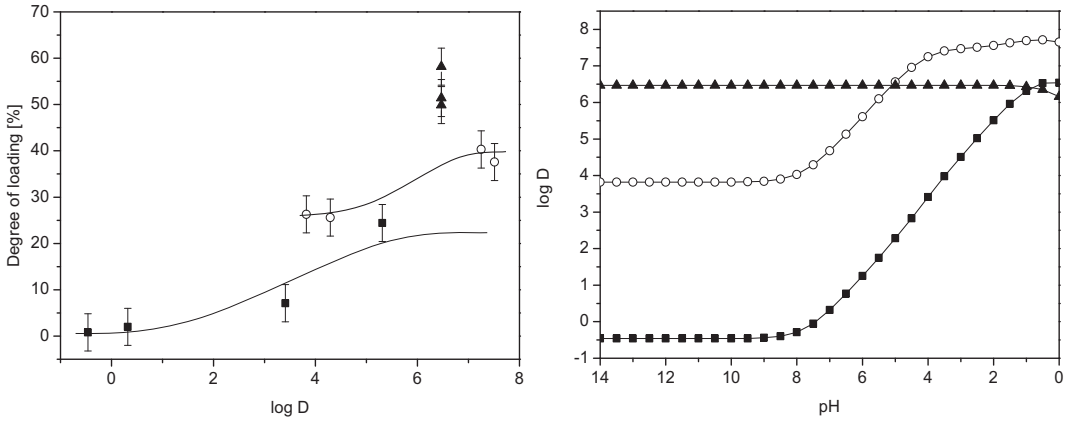

Fig. 7. Left panel: Degree of loadings of DY-750 (open circles) and DY-751 (full squares) and the control dye Itrybe (full triangles) into 100 nm-sized plain PSP. Amount of dye: 3×10^{-8} mol; 14% DMF/water. The lines are guides to the eye only. Right panel: pH-dependence of the $\log D$ values of the fluorophores.

Table 1
pH-dependence of the relative degree of dye loading of differently charged dyes incorporated into 100-nm sized PSP with various surface chemistries.

pH	Nile Red			DY-750			Itrybe		
	Carboxy-modified PSP	Amino-modified PSP	Plain PSP	Carboxy-modified PSP	Amino-modified PSP	Plain PSP	Carboxy-modified PSP	Amino-modified PSP	Plain PSP
4	45%	97%	45%	31%	68%	38%	48%	91%	50%
7.5	46%	88%	43%	33%	47%	26%	51%	80%	58%
9	54%	80%	41%	26%	45%	26%	59%	82%	52%

revealing constant log *D* values in the pH range of 4–9 and anionic DY-750 with a pH-dependent log *D* value (Fig. 7, right panel). As follows from Table 1, summarizing the results of these measurements, dye encapsulation into plain and carboxylated PSP occurs to a comparable extent. For plain PSP, the incorporation efficiency of Nile Red and Itrybe is not affected by pH whereas for DY-750, a reduction in pH from 7.5 to 4 results in an increase in the degree of dye loading by a factor of 1.5 (Fig. 7). Carboxylated PSP show improved encapsulation for Nile Red and Itrybe ($\sim$20%) at pH 9. A plausible explanation for this pH-dependence could be a widening of the polymer network due to electrostatic repulsion of the charged surface functionalities [63,64]. Contrary to the trends observed for Nile Red and Itrybe, the degree of loading of DY-750 found for carboxylated PSP at pH 9 is slightly reduced. This is attributed to electrostatic repulsion of the negatively charged dye from the negatively charged PSP surface although the effects are not very pronounced. For aminated PSP, dye incorporation is generally enhanced by a factor of 1.5–1.8 in all cases compared to carboxylated and plain PSP. This is tentatively ascribed to the different core material of the aminated PSP used here made from a polystyrene-copolymer. The degree of dye loading can be improved by at least 10% at pH 4, indicating the influence of surface charge and electrostatic repulsion also for aminated PSP.

These results confirm the suitability of log *D* values as a tool for the prediction of dye incorporation efficiency. The influence of the chemical nature and charge of the PSP surface functionalities on dye loading as shown in Table 1 is much less pronounced compared to the influence of dye charge and especially pH, controlling the hydrophobicity of fluorophores carrying (de)protonable groups as shown in Fig. 7. These findings enable further optimization of our swelling procedures and can be possibly exploited for pH-controlled tuning of dye polarity and sequential dye loading.

3.6. Zeta potential and agglomeration

One of the key factors determining the applicability of nanoparticles is their colloidal stability. The size of the zeta potential, representing the surface charge, determines too a large extent the electrostatic stabilization of the particles. Dye staining can principally affect PSP surface charge, especially in the case of charged fluorophores. The dependence of the zeta potential of dye-loaded PSP on fluorophore charge and amount of dye encapsulated is summarized in Table 2 for neutral Nile Red, cationic Itrybe, and anionic DY-750 and unloaded 1-μm sized carboxylated PSP that have a negative zeta potential of −39 mV. Incorporation of neutral molecules like Nile Red does not affect PSP zeta potential. Accordingly, PSP stained with Nile Red do not aggregate even at high dye concentrations of 3×10^{-3} mol/L (see SI, Figure 4S, right panel). Loading with anionic dyes like DY-750 decreases the zeta potential, thus increasing PSP surface charge whereas staining with a cationic dye such as Itrybe results in an increase in zeta potential, and thus, in a reduced colloidal stability, favoring dye concentration-dependent PSP agglomeration. As revealed by flow cytometry (see SI, Figure 4S, left panel; increase in FSC signal), staining of PSP with concentrations of Itrybe between 1×10^{-4} mol/L and 5×10^{-4} mol/L does not affect particle stability whereas loading with 1×10^{-3} mol/L dye results in an increased zeta potential of −18 mV, at which the particles start to form aggregates. At higher Itrybe loading, aggregation becomes more pronounced.

As the zeta potential is considerably affected by pH, especially in the case of (de)protonable groups on the surface, we investigated the influence of the pH of the surrounding medium on the zeta potential of carboxylated PSP loaded with Itrybe. As follows from Fig. 8, unstained PSP or particles exposed to Itrybe concentrations $<5 \times 10^{-4}$ mol/L have zeta potentials higher than the critical threshold of ±18 mV for agglomeration at all pH values, as indicated in Fig. 5. At a pH of 7, present in biologically relevant media, even higher loaded particles are still colloidally stable.

These findings underline the need to consider dye charge and concentration as well as pH for the tailor-made preparation of bright and stable particles. This is especially important for charged

Table 2
Staining-induced change of the zeta potential of 1 μm-sized carboxylated PSP at pH 7.

Applied dye concentration [$\times 10^{-3}$ mol/L]	Nile Red	DY-750	Itrybe
	Zeta potential [mV]	Zeta potential [mV]	Zeta potential [mV]
3	−37	–	−5
2	–	–	−7
1	–	−51	−18
0.5	–	−49	–
0.1	–	−43	−21
0.01	−32	–	−35
0	−39	−39	−39

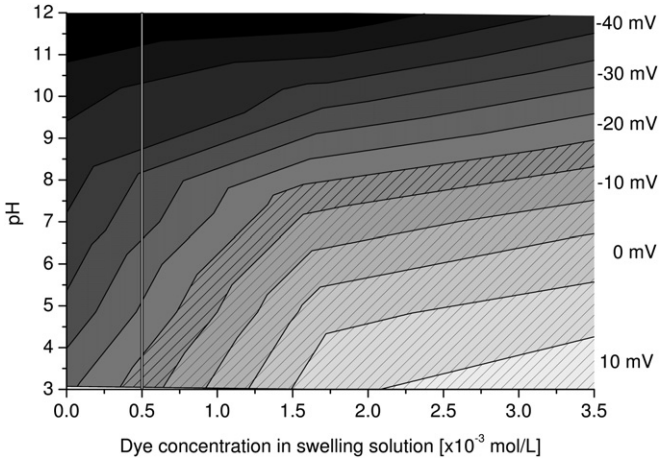

Fig. 8. Zeta potential of 1-μm sized carboxylated PSP stained with different concentrations of Itrybe as a function of pH. Zeta potentials between ±18 mV were identified by us as a critical limit for inducing agglomeration as follows from flow cytometric measurements. To highlight this critical region, these zeta potentials are indicated by pattern.

Table 3
Dye leaking studies with 1-μm sized and 100-nm sized carboxylated PSP.

	Time	Nile Red dye content	Itrybe dye content
Water	1 Year	96%	94%
HBSS/BSA	4 Weeks	93%	92%

chromophore systems that present the vast majority of NIR emitters and particles functionalized with (de)protonable groups. With this respect, the use of neutral fluorophores like coumarines or oxazines and possibly also zwitterionic dyes can be advantageous, but typically restricts particle emission to the visible region.

3.7. Leaking studies

One of the main concerns of particle staining via swelling procedures is the potential risk of dye leakage. This can reduce particle long-term stability and can be critical with respect to potential dye cytotoxicity. Main factors governing dye leaking are the polarity of the fluorophore and its solubility in the solvent or matrix surrounding the PSP. Aiming at future application of NIR fluorescent PSP, e.g. as fluorescent reporters in targeted probes for in vitro and in vivo biomarker analysis, we performed several leaking studies with 1-μm sized and 100-nm sized carboxylated PSP stained with 1×10^{-7} mol of Nile Red and Itrybe previously studied. Keeping the stained PSP in aqueous suspension for a year simulates particle storage, and storing the PSP in HBSS containing 5% BSA (HBSS/BSA) for four weeks, mimicks a biologically relevant environment. Carboxylated PSP were choosen because of their negative zeta potential assumed to improve their colloidal stability. In all cases, spectroscopic analysis of the supernatants did not provide any hint for dye leakage. Moreover, the determination of the dye content after dissolution of the particles in THF, yielding dye recovery rates of at least 92% in all cases (Table 3), underline the excellent stability of our stained particles.

3.8. Spectroscopic properties of stained PSP

The rigid and apolar PS matrix can influence the spectroscopic properties and the photochemical stability of the incorporated fluorophores, especially in the case of polarity-sensitive dyes and chromophores containing flexible double bonds where *cis–trans* isomerization acts as one of the major pathways for the non-radiative deactivation of the excited state [21,23,65,66]. Hence, we studied the absorption and fluorescence emission spectra of solvatochromic Nile Red and rather polarity-insensitive Itrybe, incorporated into PSP of various sizes (Fig. 9). The absorption spectrum of Nile Red in the 25-nm sized PSP is slightly red shifted compared to that in ethanol (Fig. 9, panel a). The shape and especially the spectral position of the emission spectra display a clear

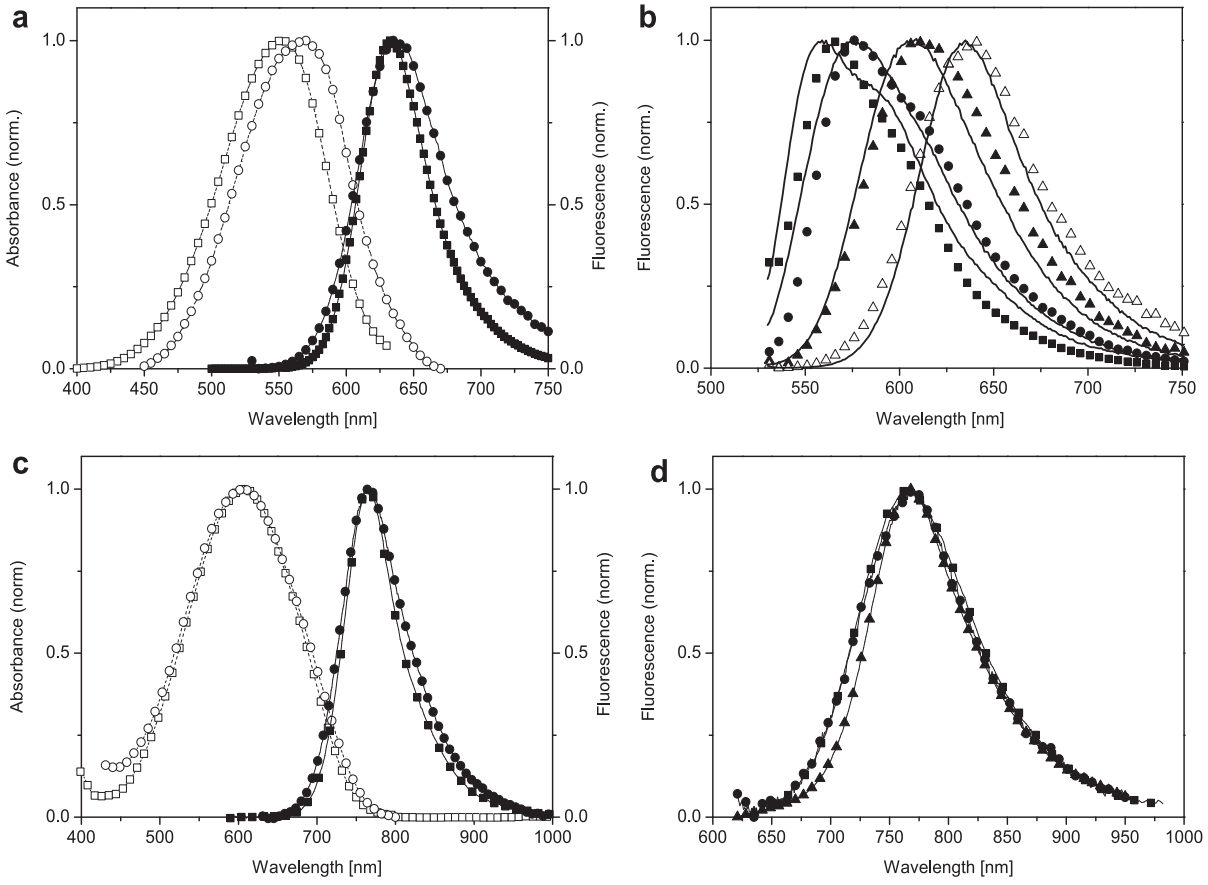

Fig. 9. (a) Normalized absorption (open symbols) and fluorescence (full symbols) spectra of Nile Red in ethanol (squares) and encapsulated in 25-nm sized PSP (circles). (b) Normalized fluorescence spectra of Nile Red encapsulated in differently sized PSP: 8 μm (full squares), 1 μm (full circles), 100 nm (full triangles), and 25 nm (open triangles). The solid lines represent the increasingly red shifted emission spectra of Nile Red in BOB, 99% BOB/1% ethanol, 90% BOB/10% ethanol, and in ethanol. Excitation of Nile Red was always at 510 nm. (c) Normalized absorption (open symbols) and fluorescence (full symbols) spectra of Itrybe in ethanol (full squares) and encapsulated in 25-nm sized PSP (full circles). (d) Normalized fluorescence spectra of Itrybe encapsulated in differently sized PSP: 1 μm (full squares), 100 nm (full circles), and 25 nm (full triangles). Excitation of Itrybe was always at 600 nm. All fluorescent PSP were obtained by staining 3 mg particles with 5×10^{-8} mol dye in 14% THF/water.

dependence on particle size, with the emission spectra being red shifted with decreasing particle size (Fig. 9, panel b). The emission spectrum of 8-μm sized stained PSP resembles the emission spectrum of Nile Red in aprotic and apolar BOB, often used as model system for PS due to the comparable polarity. The emission spectra obtained for 1-μm, 100-nm, and 25-nm sized PSP match the spectra of Nile Red in mixtures of 99% BOB/1% ethanol, 90% BOB/10% ethanol, and pure ethanol. The clear dependence of the emission maximum of Nile Red on PSP size and thus, on increasing surface-to-volume ratio of the PSP, is attributed to the increasing number of dye molecules located close to the particle surface as compared to the number of dye molecules embedded in the center of the particles. Obviously, molecules near the particle surface, although encapsulated in PS, are still affected by surrounding water molecules of the suspension, thus reporting the more polar environment by a bathochromic shift in emission. For Itrybe displaying only a very slight dependence of its spectroscopic properties on solvent polarity and proticity, the spectral position and shape of the absorption and emission bands are independent of particle size of PSP (Fig. 9, panel d) and match with the corresponding spectra obtained in ethanol (Fig. 9, panel c).

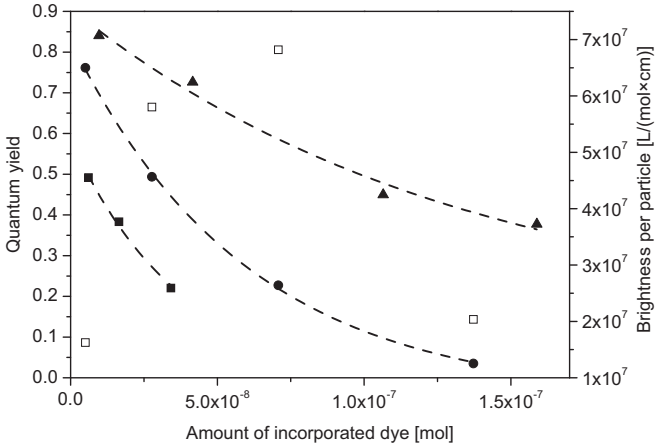

Fig. 10. Influence of the amount of incorporated dye on the fluorescence quantum yield of Nile Red encapsulated in 25-nm sized (full squares), 100-nm sized (full circles), and 1-μm sized (full triangles) carboxylated PSP and on the brightness per particle (open squares) of the 100-nm sized carboxylated PSP. The lines present a guide to the eye only.

3.9. Signal size and particle brightness

One of the most important properties of fluorescent reporters is the size of the fluorescence signal they generate. This determines the sensitivity of detection from the chromophore side. An often-used tool for the comparison of fluorophores presents the brightness, the product of the fluorescence quantum yield and the molar absorption coefficient at the excitation wavelength. In the case of nano- and micrometer-sized labels and probes, the determination of these quantities is often hampered by scattering, at least for the majority of particles with sizes exceeding ca. 25 nm that results, e.g. in an apparent size- and wavelength-dependent absorption. Accordingly, the use of common relative optical methods for the determination of the fluorometric key parameter fluorescence quantum yield becomes increasingly erroneous with increasing particle size. In addition, the molar absorption coefficient ε and the fluorescence quantum yield can be affected by dye microenvironment as well as by dye–dye interactions in a dye- and concentration-specific manner [35]. This complicates the comparison of the optical properties of encapsulated fluorophores to that of the same dye molecules in solution [20,67]. Also, there is no linear correlation to be expected between the number of fluorophores per particle and the resulting brightness, but a dye-, matrix-, and particle-size dependent maximum for a certain number of dye molecules per particle [27].

As a first step towards the assignment of brightness values to particles, we determined the absolute fluorescence quantum yield of Nile Red-stained PSP as a function of particle size and dye concentration using a custom-built integrating sphere setup. To the best of our knowledge, this is the first report on systematic studies of the absolute fluorescence quantum yields of nanometer- to micrometer-sized fluorescent particles in suspension. Nile Red was chosen here as its molar absorption coefficient is barely affected by dye environment as indicated by the relatively small differences of the ε values in polar protic ethanol ($35{,}000\ \mathrm{L\,(mol\,cm)^{-1}}$) and apolar aprotic BOB ($38{,}000\ \mathrm{L\,(mol\,cm)^{-1}}$). Moreover, Nile Red with its charge transfer-type emission is comparatively little prone to reabsorption effects and to aggregation. Its fluorescence quantum yield, however, is known to decrease with increasing polarity resulting in complete fluorescence quenching in the presence of larger amounts of water [62].

As summarized in Fig. 10, the fluorescence quantum yield of Nile Red in PSP depends on both particle size and the number of fluorophores encapsulated. The lower fluorescence quantum yields of 0.76 and especially 0.49 found for the smallest dye concentration (5×10^{-9} mol per 3 mg PSP) in 100-nm sized and 25-nm sized PSP, respectively, compared to a value of 0.84 for 1-μm sized PSP are ascribed to polarity effects [62], in agreement with the observed particle-size dependent shifts in the emission maxima (Fig. 9). For all PSP sizes, the fluorescence quantum yields decrease continuously with increasing dye concentration per particle, with the size of the diminution being PSP size dependent. This points to fluorescence quenching dye–dye interactions within the PSP. Such effects typically depend on the distance between the fluorophores. Assuming a polymer particle as compact and spherical 100-nm sized object with a volume of $5.2 \times 10^5\ \mathrm{nm^3}$ and dye molecules with negligible volume, we calculated average dye–dye distances of 3–10 nm in the particle. This first estimation is in reasonable agreement with commonly expected values for distances over which dye–dye interaction can occur [68,69].

Fig. 10 also shows the brightness B of 100-nm sized PSP stained with Nile Red. We calculated the brightness B of our particles as a function of the amount of incorporated dye according to Eq. (3).

$$B = \Phi_f \cdot \varepsilon \cdot N \tag{3}$$

Here Φ_f and ε equal the fluorescence quantum yield and molar absorption coefficient of Nile Red and N the (average) number of molecules per particle. Here we use the measured absolute fluorescence quantum yields Φ_f of PSP (Fig. 10) and a molar absorption coefficient ε of $38{,}000\ \mathrm{L\,(mol\,cm)^{-1}}$ determined in BOB for Nile Red, thereby assuming a constant ε value, regardless of the amount of dye molecules encapsulated. N was calculated from the experimentally determined overall dye concentration, the average particle size, and the particle concentration. The number of fluorophores encapsulated in these PSP varies from about 500 to 15,000 dye molecules per particle from the lowest to highest loading concentrations used.

As follows from Fig. 10, the brightness increases up to an amount of encapsulated fluorophore of ca. 7.0×10^{-8} mol in 3 mg PSP, with increasing dye concentration. Obviously, the decrease in fluorescence quantum yield of these 100-nm sized PSP by a factor of ca. 3 as compared to the lowest dye loading of 5.0×10^{-9} mol can be compensated by the increasing number of fluorophores and the resulting increase in absorption. At higher dye loading, however,

also the resulting brightness per particle decreases. In addition to these spectroscopic ensemble measurements, we performed flow cytometry studies (see SI, Figure 5S) to characterize the fluorescence intensity of the stained PSP on a single particle level. These data confirm that with increased dye loading ($>7.0 \times 10^{-8}$ mol), the emission intensity of the particles decreases.

Efficient preparation of Nile Red-stained PSP with maximum brightness requires the determination of the optimum dye loading for each particle size. Most likely, a similar optimization is required for other dyes, even if their spectroscopic properties are less sensitive to dye microenvironment as the spectroscopic features of Nile Red as the occurrence of reabsorption, aggregation, and fluorescence (self)quenching are not only concentration-dependent, yet also dye- and matrix-inherent properties [70].

4. Conclusion and outlook

Based upon a systematic comparison of different solvents (solvent composition; pH) and materials (PSP with different surface functionalities and dyes of different charge and hydrophilicity), we derived simple, mild, and versatile one-step loading procedures for the preparation of tailor-made and colloidally stable fluorescent nanometer- to micrometer-sized particles. We identified three principal strategies for dye loading via particle swelling that cover all bioanalytically relevant dye classes ranging from neutral coumarins and oxazines emitting in the visible region over zwitterionic xanthenes and squaraines to classical near-infrared emitters like cyanine dyes of different chromophore charge. Important factors governing the preparation of particles with optimum brightness include the choice of the solvent systems, loading conditions, and dye concentration, thereby considering dye-specific properties like solubility, aggregation tendency, and Stokes shift.

With the log D value providing a measure for dye hydrophobicity, we could identify a parameter that enables the prediction of dye loading behavior as a prerequisite for the rational design of bright and stable particles. In addition, our results underline the considerable influence of dye charge and loading on the colloidal stability of fluorescent particles. Moreover, based upon first measurements of the absolute fluorescence quantum yields of suspensions of dye-loaded nanoparticles of different sizes ranging from 25 nm to 1000 nm we could assign brightness values per particles. Optimum brightness requires the dye- and matrix-specific optimization of the amount of fluorophore molecules per particles as suggested by the influence of particle size and dye concentration on the absolute fluorescence quantum yields and brightness values per bead found for Nile Red, a neutral solvatochromic fluorophore not prone to dye aggregation, It remains to be shown whether such effects are less pronounced for fluorophores with optical properties barely affected by dye microenvironment that are, however, typically more prone to reabsorption effects and dye aggregation.

The versatility of our staining procedures, in conjunction with the possibility of precise control of fluorophore concentration in the particles, simultaneous or subsequent particle loading with different fluorophores, and further functionalization of the stained PSP, e.g. with biomolecules or other ligands, render these facile swelling methods very attractive for many different areas of application emerging for nanometer- to micrometer-sized particles. This includes the design of ratiometric nanosensors and bright labels for bioimaging, platforms for multiplexed analysis or barcoding applications or as standards and calibration tools for different fluorescence techniques. These strategies are especially suited for the fabrication of NIR-emissive particles as they overcome the often encountered difficulty of encapsulating chemically less stable NIR dyes. The considerably potential of our swelling procedures was only recently demonstrated for the design of a new referenced NIR-emissive nanosensor for oxygen measurements *in vitro* and *in vivo* [24].

Acknowledgements

We gratefully acknowledge financial support from the Federal Ministry of Economics and Technology (BMWI-22/06). We would also like to thank Mrs. M. Spieles for accurately technical assistance.

Appendix. Supplementary material

Supplementary material associated with this article can be found, in the online version, at doi:10.1016/j.dyepig.2012.01.021

References

[1] Seydack M. Nanoparticle labels in immunosensing using optical detection methods. Biosensors and Bioelectronics 2005;20:2454–69.
[2] Burns A, Ow H, Wiesner U. Fluorescent core-shell silica nanoparticles: towards "Lab on a Particle" architectures for nanobiotechnology. Chemical Society Reviews 2006;35(11):1028–42.
[3] Yan JL, Estevez MC, Smith JE, Wang KM, He XX, Wang L, et al. Dye-doped nanoparticles for bioanalysis. Nano Today 2007;2(3):44–50.
[4] Morgan TT, Muddana HS, Altinoglu EI, Rouse SM, Tabakovic A, Tabouillot T, et al. Encapsulation of organic molecules in calcium phosphate nanocomposite particles for intracellular imaging and drug delivery. Nano Letters 2008;8(12):4108–15.
[5] Chan CPY, Bruemmel Y, Seydack M, Sin KK, Wong LW, Merisko-Liversidge E, et al. Nanocrystal biolabels with releasable fluorophores for immunoassays. Analytical Chemistry 2004;76(13):3638–45.
[6] Wolfbeis OS. Materials for fluorescence-based optical chemical sensors. Journal of Materials Chemistry 2005;15(27-28):2657–69.
[7] Clark HA, Hoyer M, Philbert MA, Kopelman R. Optical nanosensors for chemical analysis inside single living cells. 1. Fabrication, characterization, and methods for intracellular delivery of PEBBLE sensors. Analytical Chemistry 1999;71(21):4831–6.
[8] Lee YEK, Smith R, Kopelman R. Nanoparticle PEBBLE sensors in live cells and in vivo. Annual Review of Analytical Chemistry 2009;2:57–76.
[9] Coto-Garcia AM, Sotelo-Gonzalez E, Fernandez-Arguelles M, Pereiro R, Costa-Fernandez JM, Sanz-Medel A. Nanoparticles as fluorescent labels for optical imaging and sensing in genomics and proteomics. Analytical and Bioanalytical Chemistry 2011;399(1):29–42.
[10] Mayr T, Moser C, Klimant I. Performance of fluorescent labels in sedimentation bead arrays – a comparison study. Journal of Fluorescence 2009;19(2):303–10.
[11] Borisov SM, Mayr T, Klimant I. Poly(styrene-block-vinylpyrrolidone) beads as a versatile material for simple fabrication of optical nanosensors. Analytical Chemistry 2008;80(3):573–82.
[12] Härmä H. Particle technologies in diagnostics, Technology review. TEKES, National Technology Agency; 2002. p. 126.
[13] Nolan JP, Mandy F. Multiplexed and microparticle-based analyses: quantitative tools for the large-scale analysis of biological systems. Cytomometry Part A 2006;69A(5):318–25.
[14] Stevens PW, Wang CHJ, Kelso DM. Immobilized particle arrays: coalescence of planar- and suspension-array technologies. Analytical Chemistry 2003;75(5):1141–6.
[15] Borisov SM, Klimant I. Luminescent nanobeads for optical sensing and imaging of dissolved oxygen. Microchimica Acta 2009;164(1, 2):7–15.
[16] Han MY, Gao XH, Su JZ, Nie S. Quantum-dot-tagged microbeads for multiplexed optical coding of biomolecules. Nature Biotechnology 2001;19(7):631–5.
[17] Sukhanova A, Nabiev I. Fluorescent nanocrystal-encoded microbeads for multiplexed cancer imaging and diagnosis. Critical Reviews in Oncology/Hematology 2008;68(1):39–59.
[18] Battersby BJ, Trau M. Optically encoded particles and their applications in multiplexed biomedical assays. Australian Journal of Chemistry 2007;60(5):343–53.
[19] Pregibon DC, Toner M, Doyle PS. Multifunctional encoded particles for high-throughput biomolecule analysis. Science 2007;315(5817):1393–6.
[20] Herz E, Marchincin T, Connelly L, Bonner D, Burns A, Switalski S, et al. Relative quantum yield measurements of coumarin encapsulated in core-shell silica nanoparticles. Journal of Fluorescence 2010;20(1):67–72.
[21] Saxena V, Sadoqi M, Shao J. Enhanced photo-stability, thermal-stability and aqueous-stability of indocyanine green in polymeric nanoparticulate systems. Journal of Photochemistry and Photobiology B: Biology 2004;74(1):29–38.

[22] Muddana HS, Morgan TT, Adair JH, Butler PJ. Photophysics of Cy3-encapsulated calcium phosphate nanoparticles. Nano Letters 2009;9(4):1559–66.
[23] Miletto I, Gilardino A, Zamburlin P, Dalmazzo S, Lovisolo D, Caputo G, et al. Highly bright and photostable cyanine dye-doped silica nanoparticles for optical imaging: photophysical characterization and cell tests. Dyes and Pigments 2010;84(1):121–7.
[24] Napp J, Behnke T, Fischer L, Würth C, Wottawa M, Katschinski DM, Alves D, Resch-Genger U, Schäferling M. Targeted luminescent near-infrared polymer-nanoprobes for in vivo imaging of tumor hypoxia. Analytical Chemistry 2011;83(23):9039–46.
[25] Mistlberger G, Koren K, Scheucher E, Aigner D, Borisov SM, Zankel A, et al. Multifunctional magnetic optical sensor particles with tunable sizes for monitoring metabolic parameters and as a basis for nanotherapeutics. Advanced Functional Materials 2010;20(11):1842–51.
[26] Louie AY. Multimodality imaging probes: design and challenges. Chemical Reviews 2010;110(5):3146–95.
[27] Sun GR, Berezin MY, Fan JD, Lee H, Ma J, Zhang K, et al. Bright fluorescent nanoparticles for developing potential optical imaging contrast agents. Nanoscale 2010;2(4):548–58.
[28] van Blaaderen A, Vrij A. Synthesis and characterization of colloidal dispersions of fluorescent, monodisperse silica spheres. Langmuir 1992;8:2921–31.
[29] Zhu HG, McShane MJ. Loading of hydrophobic materials into polymer particles: implications for fluorescent nanosensors and drug delivery. Journal of The American Chemical Society 2005;127(39):13448–9.
[30] Zhang R, Cherdhirankorn T, Graf K, Koynov K, Berger R. Swelling of cross-linked polystyrene beads in toluene. Microelectronic Engineering 2008;85(5,6):1261–4.
[31] Errede LA, Hanson SC. Polymer swelling. 15. swelling and deswelling studies of polystyrene liquid-systems in binary-solutions. Journal of Applied Polymer Science 1994;54(5):619–47.
[32] Liu QH, Liu J, Guo JC, Yan XL, Wang DH, Chen L, et al. Preparation of polystyrene fluorescent microspheres based on some fluorescent labels. Journal of Materials Chemistry 2009;19(14):2018–25.
[33] Bringley JF, Penner TL, Wang RZ, Harder JF, Harrison WJ, Buonemani L. Silica nanoparticles encapsulating near-infrared emissive cyanine dyes. Journal of Colloid and Interface Science 2008;320(1):132–9.
[34] Mader H, Li XH, Saleh S, Link M, Kele P, Wolfbeis OS. Fluorescent silica nanoparticles. In: Wolfbeis OS, editor. Fluorescence methods and applications: spectroscopy, imaging, and probes. Oxford: Blackwell Publishing; 2008. p. 218–23.
[35] Schobel U, Egelhaaf HJ, Brecht A, Oelkrug D, Gauglitz G. New-donor–acceptor pair for fluorescent immunoassays by energy transfer. Bioconjugate Chemistry 1999;10(6):1107–14.
[36] Natte K, Behnke T, Orts-Gil G, Würth C, Friedrich JF, Österle W, Resch-Genger U. Synthesis and characterisation of highly fluorescent core–shell nanoparticles based on Alexa dyes. Journal of Nanoparticle Research; 2012. doi:10.1007/s11051-011-0680-9.
[37] Descalzo AB, Xu HJ, Xue ZL, Hoffmann K, Shen Z, Weller MG, et al. Phenanthrene-fused boron-dipyrromethenes as bright long-wavelength fluorophores. Organic Letters 2008;10(8):1581–4.
[38] Flory PJ. Principles of polymer chemistry. Cornell University Press; 1953.
[39] Flory PI. Thermodynamics of high polymer solutions. Journal of Chemical Physics 1942;10(1):51–61.
[40] Huggins ML. Solutions of long chain compounds. Journal of Chemical Physics 1941;9(5):440.
[41] Morton M, Kaizerman S, Altier MW. Swelling of latex particles. Journal of Colloid Science 1954;9(4):300–12.
[42] Popli R. Swelling of latex-particles by water-soluble solvents. 2. Thermodynamic-equilibrium analysis. Langmuir 1991;7(1):73–80.
[43] Nemmar A, Hoylaerts MF, Hoet PHM, Dinsdale D, Smith T, Xu HY, et al. Ultrafine particles affect experimental thrombosis in an in vivo hamster model. American Journal of Respiratory and Critical Care Medicine 2002;166(7):998–1004.
[44] Brown DM, Wilson MR, MacNee W, Stone V, Donaldson K. Size-dependent proinflammatory effects of ultrafine polystyrene particles: a role for surface area and oxidative stress in the enhanced activity of ultrafines. Toxicology and Applied Pharmacology 2001;175(3):191–9.
[45] Olivier V, Duval JL, Hindie M, Pouletaut P, Nagel MD. Comparative particle-induced cytotoxicity toward macrophages and fibroblasts. Cell Biology and Toxicology 2003;19(3):145–59.
[46] Gibaud S, Demoy M, Andreux JP, Weingarten C, Gouritin B, Couvreur P. Cells involved in the capture of nanoparticles in hematopoietic organs. Journal of Pharmaceutical Sciences 1996;85(9):944–50.
[47] Clift MJD, Rothen-Rutishauser B, Brown DM, Duffin R, Donaldson K, Proudfoot L, et al. The impact of different nanoparticle surface chemistry and size on uptake and toxicity in a murine macrophage cell line. Toxicology and Applied Pharmacology 2008;232(3):418–27.
[48] Gessner A, Lieske A, Paulke BR, Muller RH. Functional groups on polystyrene model nanoparticles: influence on protein adsorption. Journal of Biomedical Materials Research: Part A 2003;65A(3):319–26.
[49] Sun XK, Rossin R, Turner JL, Becker ML, Joralemon MJ, Welch MJ, et al. An assessment of the effects of shell cross-linked nanoparticle size, core composition, and surface PEGylation on in vivo biodistribution. Biomacromolecules 2005;6(5):2541–54.
[50] Qian HS, Li ZQ, Zhang Y. Multicolor polystyrene nanospheres tagged with upconversion fluorescent nanocrystals. Nanotechnology 2008;19(25):4.
[51] Li MJ, Zhang H, Zhang JH, Wang CL, Han K, Yang B. Easy preparation and characterization of highly fluorescent polymer composite microspheres from aqueous CdTe nanocrystals. Journal of Colloid and Interface Science 2006;300(2):564–8.
[52] Zhang Q, Han Y, Wang WC, Zhang L, Chang J. Preparation of fluorescent polystyrene microspheres by gradual solvent evaporation method. European Polymer Journal 2009;45(2):550–6.
[53] Borisov SM, Herrod DL, Klimant I. Fluorescent poly(styrene-block-vinylpyrrolidone) nanobeads for optical sensing of pH. Sensors and Actuators B: Chemical 2009;139(1):52–8.
[54] Behnke T, Würth C, Hoffmann K, Hübner M, Panne U, Resch-Genger U. Encapsulation of hydrophobic dyes in polystyrene micro- and nanoparticles via swelling procedures. Journal of Fluorescence 2011;21(3):937–44.
[55] Resch-Genger U, Pfeifer D, Monte C, Pilz W, Hoffmann A, Spieles M, et al. Traceability in fluorometry: Part II. Spectral fluorescence standards. Journal of Fluorescence 2005;15(3):315–36.
[56] Würth C, Lochmann C, Spieles M, Pauli J, Hoffmann K, Schuttrigkeit T, et al. Evaluation of a commercial integrating sphere setup for the determination of absolute photoluminescence quantum yields of dilute dye solutions. Applied Spectroscopy 2010;64(7):733–41.
[57] Würth C, Grabolle M, Pauli J, Spieles M, Resch-Genger U. Comparison of methods and achievable uncertainties for the relative and absolute measurement of photoluminescence quantum yields. Analytical Chemistry 2011;83(9):3431–9.
[58] Hunter RJ. Zeta potential in colloid science: principles and applications. London: Academic Press; 1981.
[59] Deye JF, Berger TA, Anderson AG. Nile Red as a solvatochromic dye for measuring solvent strength in normal liquids and mixtures of normal liquids with supercritical and near critical fluids. Analytical Chemistry 1990;62(6):615–22.
[60] Golini CM, Williams BW, Foresman JB. Further solvatochromic, thermochromic, and theoretical studies on Nile Red. Journal of Fluorescence 1998;8(4):395–404.
[61] Jee AY, Park S, Kwon H, Lee M. Excited state dynamics of Nile Red in polymers. Chemical Physics Letters 2009;477(1–3):112–5.
[62] Greenspan P, Fowler SD. Spectrofluorometric studies of the lipid probe, Nile Red. The Journal of Lipid Research 1985;26(7):781–9.
[63] Kratz K, Hellweg T, Eimer W. Influence of charge density on the swelling of colloidal poly(N-isopropylacrylamide-co-acrylic acid) microgels. Colloids and Surfaces A: Physicochemical and Engineering Aspects 2000;170(2, 3):137–49.
[64] Pan SH, Conway V, Shakhsher Z, Emerson S, Bai MQ, Seitz WR, et al. Mechanically robust amine derivatized polystyrene for Ph sensing based on polymer swelling. Analytica Chimica Acta 1993;279(2):195–202.
[65] Herz E, Ow H, Bonner D, Burns A, Wiesner U. Dye structure-optical property correlations in near-infrared fluorescent core-shell silica nanoparticles. Journal of Materials Chemistry 2009;19(35):6341–7.
[66] Sokolov I, Naik S. Novel fluorescent silica nanoparticles: towards ultrabright silica nanoparticles. Small 2008;4(7):934–9.
[67] Schwartz A, Wang L, Early E, Gaigalas A, Zhang YZ, Marti GE, et al. Quantitating fluorescence intensity from fluorophore: The definition of MESF assignment. Journal of Research of the National Institute of Standards and Technology 2002;107(1):83–91.
[68] Johansson MK, Cook RM. Intramolecular dimers: a new design strategy for fluorescence-quenched probes. Chemistry – A European Journal 2003;9(15):3466–71.
[69] Nooney RI, McCahey CMN, Stranik O, Guevel XL, McDonagh C, MacCraith BD. Experimental and theoretical studies of the optimisation of fluorescence from near-infrared dye-doped silica nanoparticles. Analytical and Bioanalytical Chemistry 2009;4(393):1143–9.
[70] Resch-Genger U, Grabolle M, Cavaliere-Jaricot S, Nitschke R, Nann T. Quantum dots versus organic dyes as fluorescent labels. Nature Methods 2008;5(9):763–75.